Smart Structures and Systems, *Vol. 20, No. 2 (2017) 139-150*
DOI: https://doi.org/10.12989/sss.2017.20.2.139

Strain-based structural condition assessment of an instrumented arch bridge using FBG monitoring data

X.W. Ye[1a], Ting-Hua Yi[*2], Y.H. Su[1b], T. Liu[1c] and B. Chen[1d]

[1]*Department of Civil Engineering, Zhejiang University, Hangzhou 310058, China*
[2]*School of Civil Engineering, Dalian University of Technology, Dalian 116023, China*

(Received December 29, 2016, Revised April 10, 2017, Accepted April 14, 2017)

Abstract. The structural strain plays a significant role in structural condition assessment of in-service bridges in terms of structural bearing capacity, structural reliability level and entire safety redundancy. Therefore, it has been one of the most important parameters concerned by researchers and engineers engaged in structural health monitoring (SHM) practices. In this paper, an SHM system instrumented on the Jiubao Bridge located in Hangzhou, China is firstly introduced. This system involves nine subsystems and has been continuously operated for five years since 2012. As part of the SHM system, a total of 166 fiber Bragg grating (FBG) strain sensors are installed on the bridge to measure the dynamic strain responses of key structural components. Based on the strain monitoring data acquired in recent two years, the strain-based structural condition assessment of the Jiubao Bridge is carried out. The wavelet multi-resolution algorithm is applied to separate the temperature effect from the raw strain data. The obtained strain data under the normal traffic and wind condition and under the typhoon condition are examined for structural safety evaluation. The structural condition rating of the bridge in accordance with the AASHTO specification for condition evaluation and load and resistance factor rating of highway bridges is performed by use of the processed strain data in combination with finite element analysis. The analysis framework presented in this study can be used as a reference for facilitating the assessment, inspection and maintenance activities of in-service bridges instrumented with long-term SHM system.

Keywords: structural heath monitoring; arch bridge; strain-based structural condition assessment; structural rating; wavelet multi-resolution algorithm; finite element analysis

1. Introduction

It is crucial to ensure that the bridge structures are operated in the specified tolerance and safe range. In the past few decades, the structural health monitoring (SHM) technology has been extensively adopted to track the structural parameters (e.g., strain, acceleration, displacement, etc.) in a continuous and real-time manner (Ni *et al.* 2010, Ni *et al.* 2012b, Ye *et al.* 2012, Ye *et al.* 2013, Ye *et al.* 2014, Ye *et al.* 2016a,b,c, Ye *et al*. 2017). In addition, with the development of innovative sensing and information processing technologies, the SHM systems for various types of civil infrastructures are emerged to identify the structural damage extent, evaluate the structural safety condition, and estimate the remaining service life. Up to now, a considerable number of SHM systems have been installed on large-scale engineering structures all over the world (Fuhr *et al.* 1999, Tennyson *et al*. 2001, Chan *et al*. 2006, Li *et al.* 2006, Jiang *et al*. 2010).

With the aid of an instrumented SHM system, multifarious monitoring parameters reflecting the global or local structural properties of the target structure can be obtained to facilitate the assessment of structural health condition and the establishment of inspection and maintenance scheme. Amongst the newly-developed cutting-edge sensing approaches, the optical fiber sensing technology has gained increasing attentions by the researchers and engineers in the field of civil engineering (Casas *et al*. 2003, Mehrani *et al.* 2009, Xiong *et al.* 2012). The monitoring items can be readily related to the optical characteristics by different types of demodulation methods such as interferometry, time domain reflectometry, and frequency domain reflectometry. Instrumentation of bridges using diversified optical fiber sensors have been widely reported in the currently-available literature (Zhang *et al.* 2006, Kister *et al*. 2007a,b, Barbosa *et al*. 2008, Costa and Figueiras 2012, Rodrigues *et al.* 2012, Surre *et al.* 2013).

In recent years, a critical issue on efficient analysis of massive monitoring data for structural condition assessment has been greatly concerned by the bridge engineers and managers. The structural strain plays a significant role in structural condition assessment of in-service bridges in terms of structural bearing capacity, structural reliability level and entire safety redundancy. Many strain-based assessment methods have been proposed and applied to

*Corresponding author, Professor
E-mail: yth@dlut.edu.cn
[a] Associate Professor
E-mail: cexwye@zju.edu.cn
[b] Ph.D. Student
[c] MSc Student
[d] Ph.D. Student

ISSN: 1738-1584 (Print), 1738-1991 (Online)

Fig. 1 Jiubao Bridge

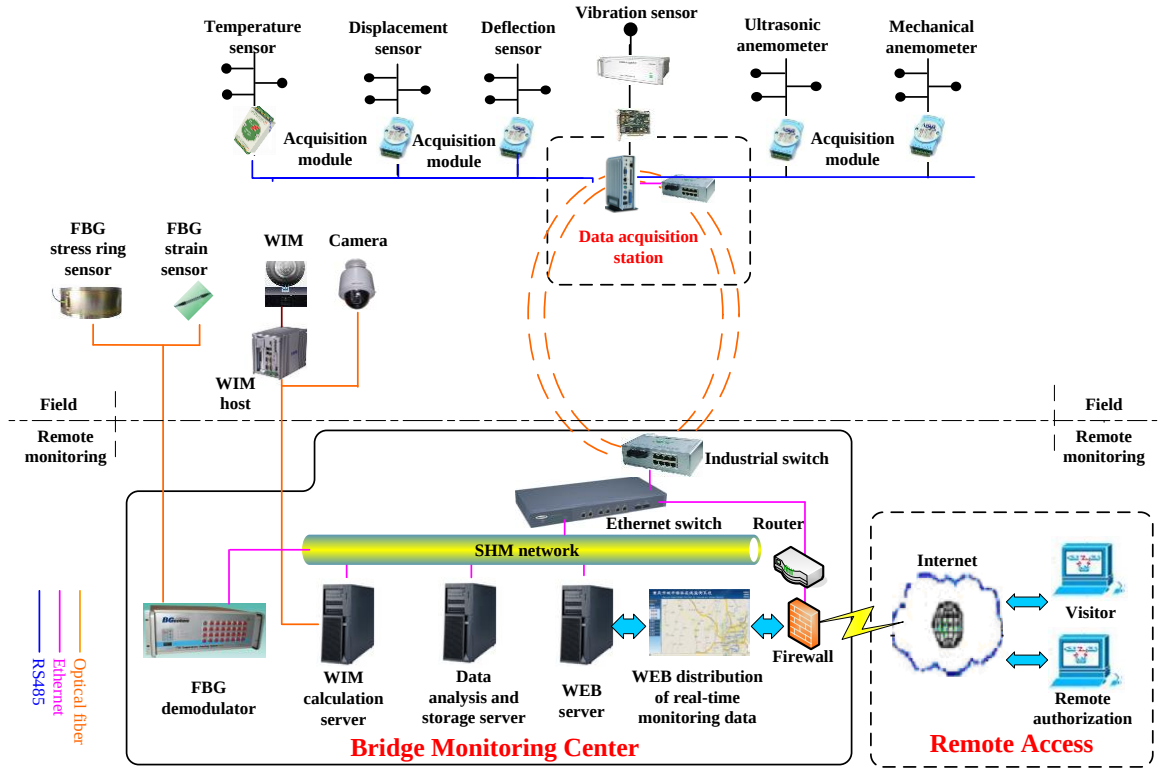

Fig. 2 SHM system of Jiubao Bridge

evaluate in-service structural performance of bridge structures (Cardini and DeWolf 2008, Ni *et al.* 2012a). In this paper, an SHM system instrumented on a composite arch bridge is introduced. The arrangement of the fiber Bragg grating (FBG)-based sensing system is highlighted. Long-term monitoring data from the FBG-based strain sensors are acquired for further analysis. A wavelet-based nonparametric approach is used to decompose the strain ingredients by multi-resolution analysis to achieve the live load-induced stress component. The structural safety condition of selected components of the bridge is evaluated by use of the strain monitoring data. Structural condition rating of the bridge in accordance with the AASHTO specification is performed by use of the processed strain data in combination with finite element analysis.

2. Structural health monitoring of Jiubao Bridge

2.1 Brief introduction of Jiubao Bridge

The Jiubao Bridge with an overall length of 1,855 m is a steel-concrete composite arch bridge located in Hangzhou, China. As illustrated in Fig. 1, this bridge consists of three main parts, the south approach spans, the main navigation channel spans, and the north approach spans. The south approach spans (90 m+9×85 m+55 m) and the north approach spans (55 m+2×85 m+90 m) are comprised of constant cross-section reinforced concrete continuous box girders. The main navigation channel spans (210 m+210 m+210 m) contain three spans of steel arch composite structures. The main spans are composed by constant cross-section continuous steel box beams and concrete deck slabs.

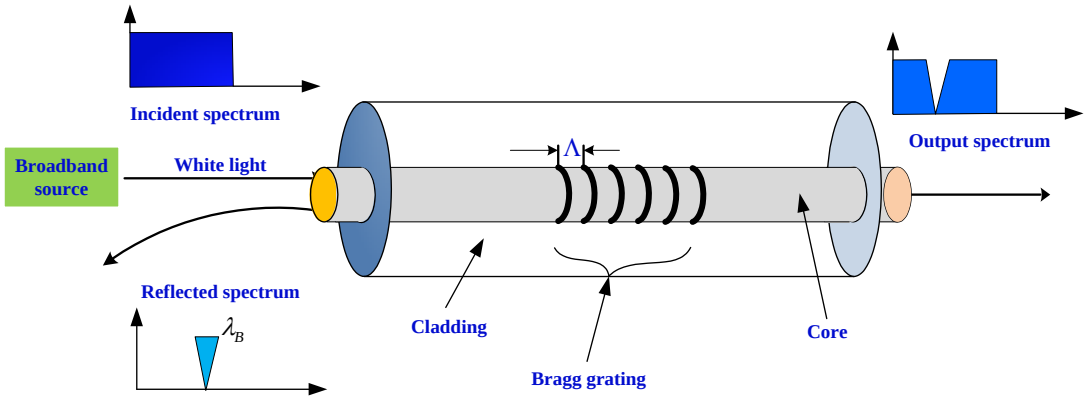

Fig. 3 Principle of FBG sensor

It was opened to the traffic in July 2012 and represents the first river-crossing bridge composed by the composite structure in full length. The bridge deck is constructed in terms of urban bridge standard of China with six traffic lanes and double-sided pavements. The design velocity of vehicle is 80 km/h.

2.2 Structural health monitoring system

After the completion of its construction, the Jiubao Bridge has been instrumented with a long-term SHM system comprising nine sophisticated subsystems (Zhou *et al*. 2016), as illustrated in Fig. 2. The real-time monitoring data are acquired through various types of sensors, including wind velocity and direction, environmental temperature and humidity, vehicle velocity and traffic volume, structural vibration, structural temperature, structural strain, alignment, displacement of bearing, and cable force.

The huge amounts of field monitoring data are collected by data acquisition stations and then transferred to bridge monitoring center for further analysis. In the monitoring center, the tasks of data storage and analysis are performed by means of specific hardware and software. The SHM system is designed to connect to the internet, and administrators and authorized visitors can easily access to the server in the monitoring center for data extraction.

The data collection and transmission subsystem consists of data acquisition stations, server clusters, and optical fiber signal transmission networks. It plays the role of data transportation from the sensor subsystem. It transfers the signals measured by the sensors to the data processing and control subsystem. In the data processing and control subsystem, the pretreated signals are processed to obtain the effective information or mechanics indices. Then, they will be delivered to the structural state and safety evaluation subsystem. The data processing and control subsystem also realizes the function of data query by the bridge administrator.

The SHM system of the Jiubao Bridge is designed and implemented to monitor the structural responses and assess the structural safety under the action of dead load, live load (highway traffic and wind), accidental load (earthquake and ship collision), and environmental load (temperature). The sensor subsystem collecting continuous original monitoring data is the basic ingredient of the SHM system. It detects and acquires structural responses and input signals (e.g., displacement, strain, acceleration, temperature, etc.) of the bridge under all kinds of excitation and environmental conditions. The arrangement points of sensors are determined through finite element analysis by the designer of the SHM system.

2.3 FBG-based strain sensors

Over the past few years, increasing attentions have been paid to the FBG sensors. An FBG can be regarded as a type of optical fiber sensor with varied refractive index in the core (Hill *et al*. 1978). As illustrated in Fig. 3, according to the Bragg's law, a beam of white light is written in an FBG sensor, and when light from broadband source passes through the grating at a particular wavelength, the Bragg wavelength, which is related to the grating period, is reflected. The Bragg wavelength λ_B can be achieved by

$$\lambda_B = 2n_{\text{eff}}\Lambda \tag{1}$$

where n_{eff} is the effective index of refraction, and Λ is the grating period. The wavelength shift changes linearly with both strain and temperature. When the grating part is subjected to external disturbance, the period of grating will be changed, and the Bragg wavelength changes accordingly.

The variation of the Bragg wavelength can be obtained by

$$\Delta\lambda_B = \lambda_B\{(\alpha_f + \xi_f)\Delta T + (1 - p_e)\varepsilon\} \tag{2}$$

where ε is the strain, ΔT is the temperature change, α_f is the coefficient of thermal expansion, ξ_f is the thermo-optic coefficient, and p_e is the strain-optic coefficient. The FBG sensor can be regarded as a type of optical fiber sensor with periodic changes of the refractive index that are formed when exposed to an intense UV interference pattern in the core of an optical fiber. Since both the axial strain and temperature cause the shift of Bragg wavelength, the temperature compensation must be carried out when using the FBG strain sensor to monitor the change of structural strain/stress.

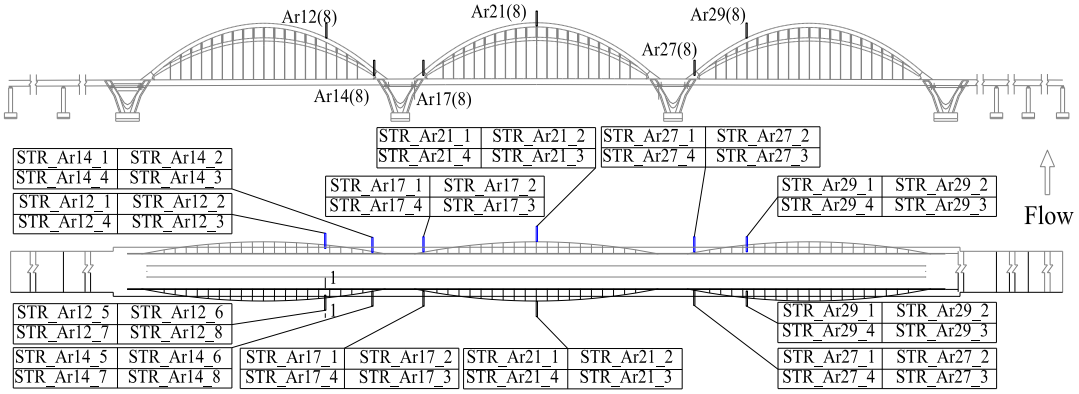

Fig. 4 Deployment of FBG-based strain sensors on arch ribs

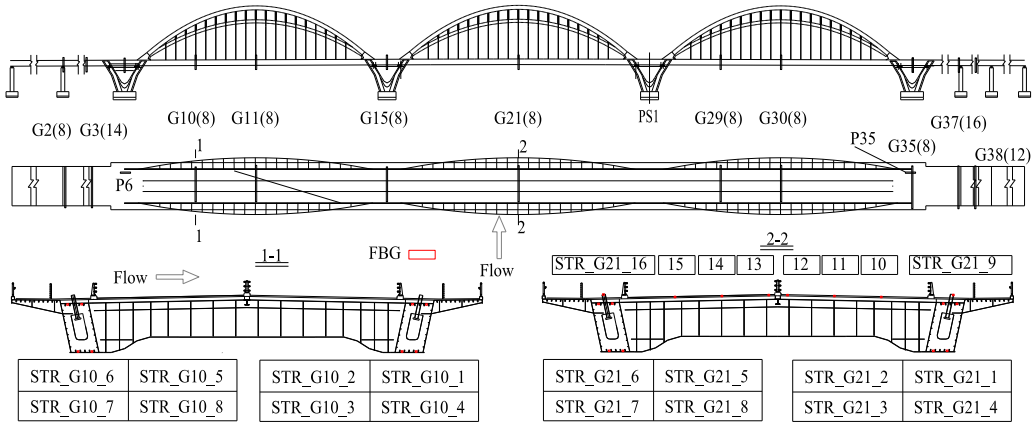

Fig. 5 Deployment of FBG-based strain sensors on girders and piers

Fig. 6 Installed FBG-based sensor

In the SHM system of the Jiubao Bridge, the FBG sensor system consists of two types of sensors including the FBG-based strain sensors and FBG-based temperature sensors. The FBG-based strain and temperature sensors are installed to monitor the stress change and fatigue damage of steel box girders and arch ribs. It should be noticed that the FBG-based temperature sensors are deployed adjacent to the FBG-based strain sensors for compensating the effect of temperature. In the data acquisition and transmission subsystem, the wavelength data collected by the FBG-based sensors are classified and transferred to the data processing and control subsystem. In the data processing and control subsystem, the stress state of structural components are analyzed, and then moved to the structural health status evaluation subsystem. In this subsystem, the evaluation of the structural condition is carried out to help the bridge managers make the optimal inspection and maintenance plans. For the structural strain monitoring, 166 measurement points in total are determined and arranged by finite element analysis, as illustrated in Figs. 4 and 5. Fig. 6 shows the field installed FBG-based sensor.

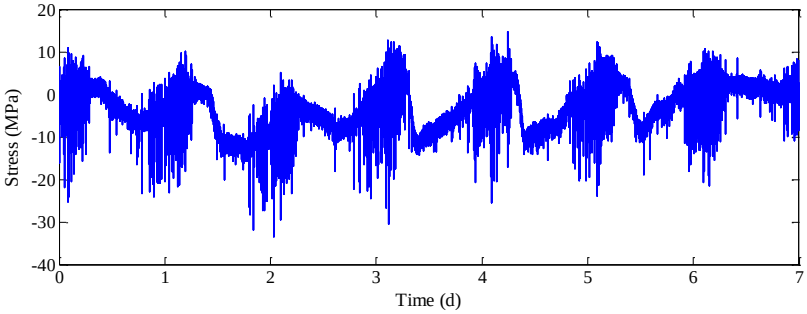

Fig. 7 Typical stress time history in one week

2.4 FBG-based strain monitoring data

After obtaining the strain monitoring data from the FBG-based sensors, the stress time histories can be derived from the acquired strain data by simply multiplying the elasticity modulus of steel. The steel grade is Q345 and the elasticity modulus is 206 GPa. Fig. 7 shows the relative variation of structural stress in one week (1 February 2016 to 7 February 2016) of the FBG strain senor STR_G11_3 deployed in the steel box girder. The strain signal collected at 00:00 am on 1 February 2016 is taken as the baseline data. It is observed from Fig. 7 that the stress time history has a periodic variation characteristic with a period of one day. It should be noted that the strain monitoring data acquired from the sensors deployed on the girders and arch ribs are mainly induced from three effects: highway traffic, wind and temperature (The static strain attributable to initial dead load cannot be obtained because the FBG sensors were installed after the completion of construction of the bridge).

As reflected by the stress time history, it is composed of low frequency signals and high frequency signals which may be caused by different kinds of factors (Ni *et al*. 2012a). The bridge girder mainly behaves as expanding or contracting along the longitudinal direction under the temperature effect. In contrast, the bridge deck undergoes flexural bending under highway traffic load. These two types of distinct responses are mixed in the strain monitoring data. It is desirable to characterize them separately when each effect on the structural behavior is required to be quantified. The extraction of a specific effect is not easy when the measured signals are non-stationary and non-Gaussian noisy in nature. A wavelet-based nonparametric approach is used to decompose the strain ingredients by multi-resolution analysis.

3. Decomposition of multi-source strain data

3.1 Wavelet multi-resolution algorithm

Transform-domain processing of a signal involves mapping it from the signal space to the transform space using a set of basis functions. For a wavelet transform, a particular function is chosen as a mother wavelet and a family of daughter wavelets is defined by scaling and shifting, serving as a complete set of basis functions. In the wavelet-based multi-resolution analysis, the same function can be adopted and repeated with different scale and shift parameters. Multi-resolution analysis is a process of choosing a set of basis functions that originate from the same mother wavelet. From a practical point of view, a wavelet multi-resolution analysis allows a decomposition of the signal into various resolution scales: the data with coarse resolution contain the information about low-frequency components, and the data with fine resolution contain the information about high-frequency components (Xia *et al*. 2012).

Using a selected mother wavelet function, $\Psi(t)$, the continuous wavelet transform of a signal is defined as

$$W_\Psi f(a,b) = \langle f, \Psi_{a,b} \rangle = \frac{1}{|a|^{1/2}} \int_{-\infty}^{\infty} f(t) \overline{\Psi}\left(\frac{t-b}{a} \right) dt, \quad a > 0 \tag{3}$$

where $\Psi(t)$ is the mother wavelet, a is a scale parameter, and b is a time parameter. The overbar represents complex conjugation. It is known that the function $f(t)$ can be reconstructed from $W_\Psi f(a,b)$ by the double-integral representation as represented by

$$f(t) = \frac{1}{C_\Psi} \int_{-\infty}^{\infty} \int_{-\infty}^{\infty} W_\Psi f(a,b) \Psi\left(\frac{t-b}{a} \right) \frac{1}{a^2} da db \tag{4}$$

In practical signal processing, a discrete version of the wavelet transform is often employed by discretizing the scale parameter, a and the time parameter, b. In general, the procedure becomes much more efficient if dyadic values of a and b are used. That is

$$a = 2^j, b = 2^j k, \; j, k \in Z \tag{5}$$

where Z is a set of positive integers. With some special choices of $\Psi(t)$, the corresponding discretized wavelets, $\{\Psi_{j,k}\}$ are expressed by

$$\Psi_{j,k}(t) = 2^{j/2} \Psi\left(2^j t - k \right) \tag{6}$$

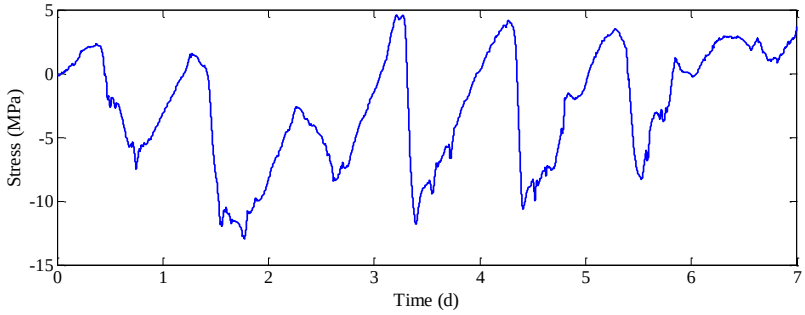

(a) Low-frequency part

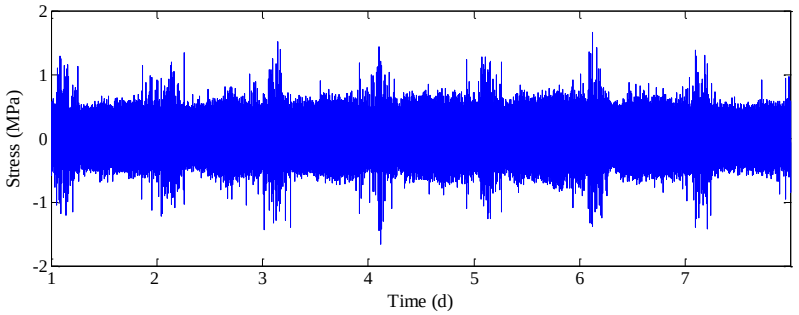

(b) High-frequency part

Fig. 8 Wavelet-based decomposed stress data

It constitutes an orthonormal basis for $L_2(R)$. With this orthonormal basis, the wavelet expansion of a function $f(t)$ can be obtained as

$$f(t)=\sum_j\sum_k \alpha_{j,k}\Psi_{j,k}(t) \tag{7}$$

where

$$\alpha_{j,k}=\int_{-\infty}^{\infty} f(t)\Psi_{j,k}dt \tag{8}$$

In the discrete wavelet analysis, a signal can be represented by its approximations and details. The detail at level j is defined as

$$D_j=\sum_{k\in Z}\alpha_{j,k}\Psi_{j,k}(t) \tag{9}$$

and the approximation at level J is defined as

$$A_J=\sum_{j>J} D_j \tag{10}$$

It follows that

$$f(t)=A_J+\sum_{j\le J} D_j \tag{11}$$

Eq. (11) provides a tree-structure decomposition of a signal and a reconstruction procedure as well. By selecting different dyadic scales, a signal can be broken down into numerous low-resolution components.

3.2 Separation of temperature effect

Fig. 8 illustrates the wavelet-based decomposed stress time histories of the FBG strain senor STR_G11_3 in one week (1 February 2016 to 7 February 2016). The low-frequency parts of 12-level decomposition of stress data represent the reconstructed temperature-induced stress component. It indicates that the temperature-induced stress time history has a similar variation tendency and periodic characteristic with a daily stress data. The temperature-induced stress takes major part of the total stress which means that the main stress change during the bridge operational status is caused by the temperature effect. Also, Fig. 8 shows the high-frequency parts of 12-level decomposition of stress data which consist of live load (highway traffic and wind) induced stress component. The stress amplitudes vary approximately within 2 MPa, indicating that the live load-induced stress is taking a minor part of the total stress. Fig. 9 illustrates the stress time histories of the FBG strain sensor STR-G11-5 at the top plate and the FBG strain sensor STR-G11-8 at the bottom plate of mid-span section on 22 February 2016.

3.3 Analysis of daily strain data under typhoon

It is crucial for bridge engineers and managers to check the stress level of key bridge components under extreme weather condition for structural serviceability and safety evaluation. Since the operation of the Jiubao Bridge, the bridge has been attacked by several typhoons. The Typhoon Soudelor is the second most intense tropical cyclone

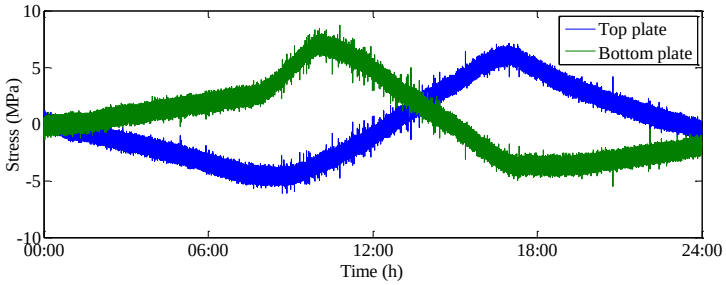

(a) Daily stress time histories

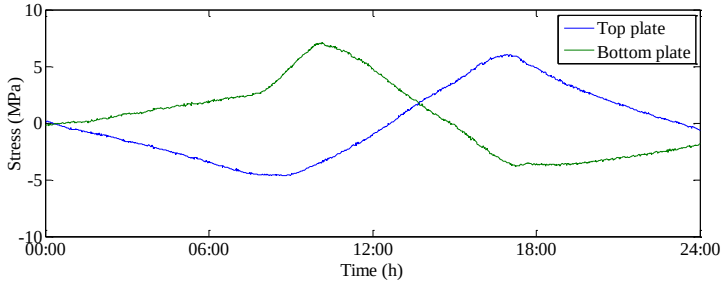

(b) Temerature-induced stress time histories

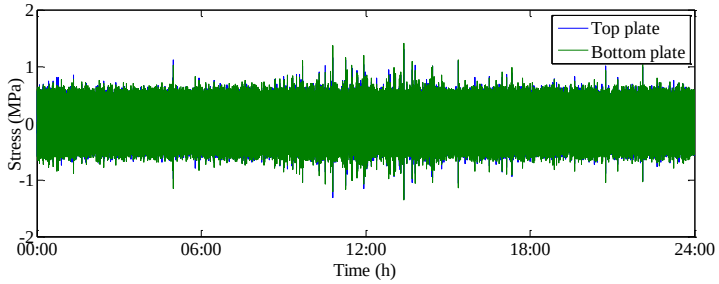

(c) Live load-induced stress time histories

Fig. 9 Stress time histories of top and bottom plates at mid-span section

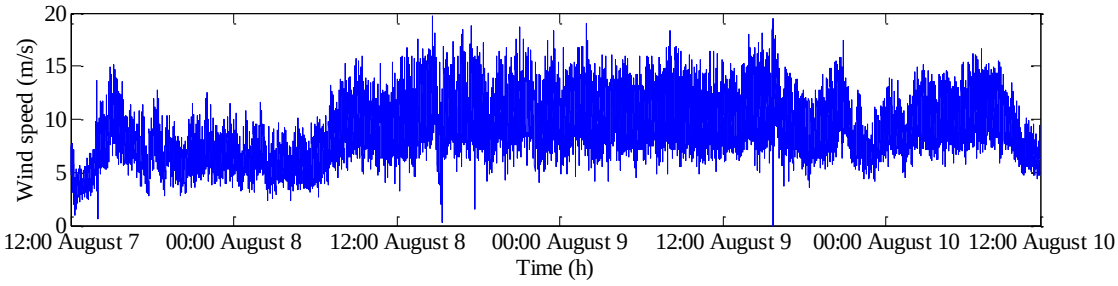

(a) Wind speed

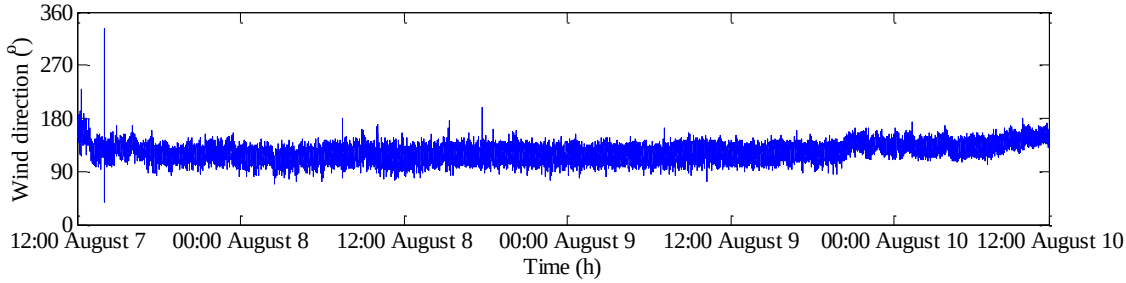

(b) Wind direction

Fig. 10 Measured wind data during Typhoon Soudelor

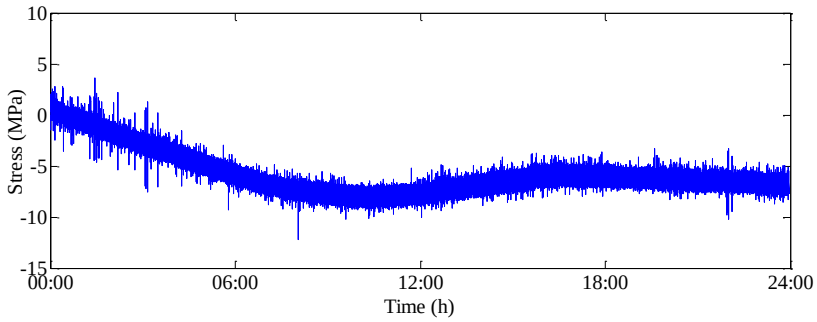

(a) Daily stress time history

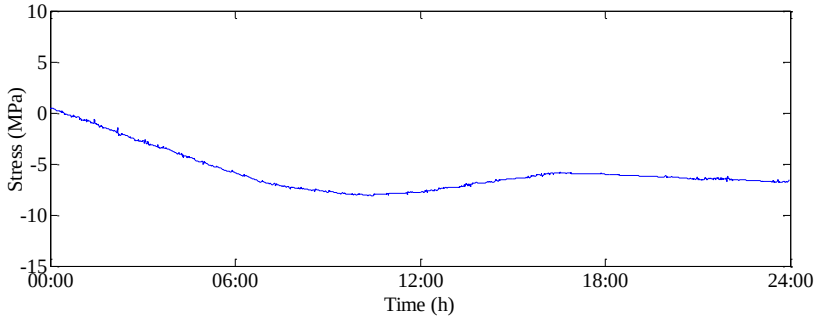

(b) Temerature-induced stress time history

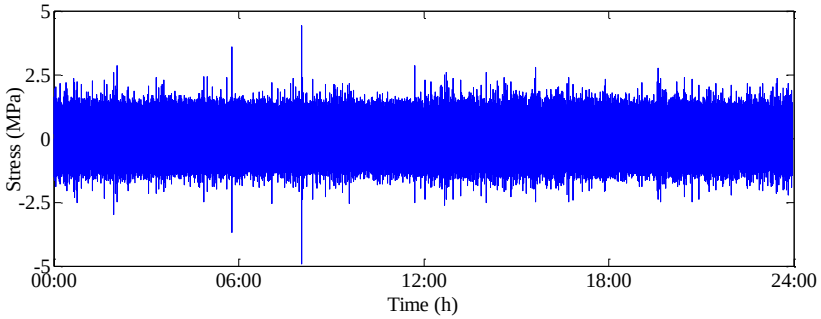

(c) Live load-induced stress time history

Fig. 11 Stress time history under typhoon on 9 August 2015

worldwide in 2015 as well as the strongest tropical cyclone of the 2015 Pacific typhoon season. It had caused severe impacts in the Northern Mariana Islands, Taiwan, and eastern China, resulting in 40 confirmed fatalities. It moved inland over eastern China and was degraded to a tropical depression on 9 August 2015. Fig. 10 illustrates the wind data collected by the anemometer during Typhoon Soudelor. Fig. 11 shows the stress time history under typhoon measured by the FBG strain senor STR-G11-7 on 9 August 2015 as well as the decomposed stress components caused by the live load and temperature. It is seen from Fig. 11 that the live load-caused stress fluctuation range is approximately within 5 MPa, which is relative larger than that measured in common days.

4. Strain-based structural condition rating

The arithmetic expression for structural condition rating of bridges provided in AASHTO specification for condition evaluation and load and resistance factor rating of highway bridges (AASHTO 2011) is defined as

$$RF = \frac{C - (\gamma_{DC})(DC) - (\gamma_{DW})(DW) \pm (\gamma_P)(P)}{(\gamma_{LL})(LL + IM)} \quad (12)$$

where RF is the rating factor, C is the flexural capacity of the beam, DC is the dead load effect of the beam due to structural components and attachments, DW is the dead load effect due to wearing surfaces and utilities, P is the permanent loads other than dead loads, LL is the live load effect, IM is the dynamic load allowance, γ_{DC} is the LRFD load factor for structural components and attachments, γ_{DW} is the LRFD load factor for wearing surfaces and utilities, γ_P is the LRFD load factor for permanent loads other than dead loads, and γ_{LL} is the live load factor. The flexural capacity of the beam can be calculated by

For the strength limit state

$$C = \varphi_C \varphi_S \varphi R_N \quad (13)$$

Table 1 Element type and number of structural component

Structural component	Element type	Number
Main arch	Beam element	132
Sub arch	Beam element	120
Cable	Tension-only element	114
Girder	Beam element	414
Stringer	Beam element	284
Crossbeam	Beam element	572
Deck	Plate element	568
Tied cable	Tension-only element	16
Brace	Beam element	9
Link	Beam element	102

Table 2 Material parameters of finite element model

Material	Elasticity modulus (MPa)	Unit weight (kN/m^3)	Poisson's ratio	Expansion coefficient (/℃)
Concrete (C50)	3.45E+4	26	0.2	1.0E-5
Steel wire	2.06E+5	78.5	0.3	1.2E-5
High tensile steel wire	1.90E+5	78.5	0.3	1.2E-5
External cable	1.90E+5	78.5	0.3	1.2E-5

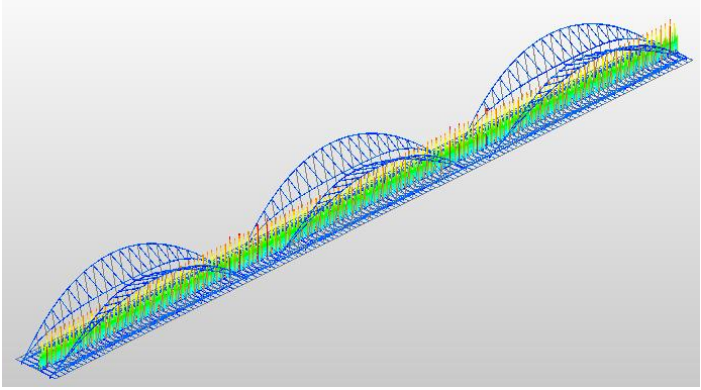

Fig. 12 Finite element model of Jiubao Bridge

$$\varphi_C \varphi_S \geq 0.85 \tag{14}$$

For the service limit state

$$C = f_R \tag{15}$$

where φ_C is the condition factor, φ_S is the system factor, φ is the LRFD resistance factor, R_N is the nominal resistance, and f_R is the allowable stress specified in the LRFD code. For the structural condition rating of the beam at the inventory rating level as specified in AASHTO (2011), the above-mentioned rating parameters are determined as γ_{DC}=1.25, γ_{DW}=1.5, γ_P=1, γ_{LL}=1.75, IM=0.33×LL, φ_C=1, φ_S=1, and φ=1.

In accordance of Eq. (12), the dead load effect due to structural components and attachments and the dead load effect due to wearing surfaces and utilities are unknown parameters while the live load effect can be derived by the monitoring data for the strength limit state. For a specific structural component deployed with the FBG strain sensor, the strain component caused by the live load can be extracted by the proposed wavelet multi-resolution analysis through decomposing the temperature effect from the stress time history. In this study, in order to determine the dead load effect of the investigated structural component, a finite element model of the Jiubao Bridge is constructed, as shown in Fig. 12. The detailed information of the element type, element number and material parameter of structural component are listed in Table 1 and Table 2. The results of calculated stress values of selected sensor positions by finite element analysis are listed in Table 3.

After obtaining the dead load effect by finite element analysis and the live load effect from the strain monitoring data processed by wavelet multi-resolution analysis, the rating factor of an instrumented structural component can be calculated. Fig. 13 shows the daily rating factor of the structural component where the FBG strain sensor STR-11-7 installed under different load conditions (weekday heavy traffic condition, weekend light traffic condition, and typhoon condition). It can be observed from Fig. 13 that the rating factor values are much more than 1, indicating that the structural component is operated in a safe condition.

Table 3 Stress values of quarter-span and mid-span sections

Parameter	Stress (MPa)							
	Quarter-span section				Mid-span section			
	STR-G10-5	STR-G10-6	STR-G10-7	STR-G10-8	STR-G11-5	STR-G11-6	STR-G11-7	STR-G11-8
DC	-40.2MPa	-39.3MPa	67.6MPa	63.2MPa	-49.3MPa	-42.3MPa	68.1MPa	63.8MPa
DW	-8.4MPa	-8.0MPa	12.5MPa	10.5MPa	-10.1MPa	-9.6MPa	14.2MPa	11.2MPa
R_N	295MPa							

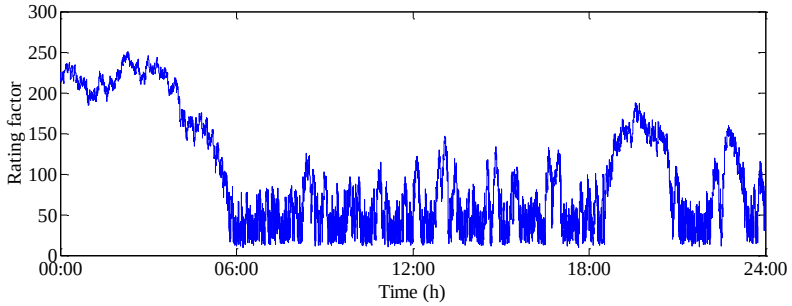

(a) Under weekday heavy traffic condition

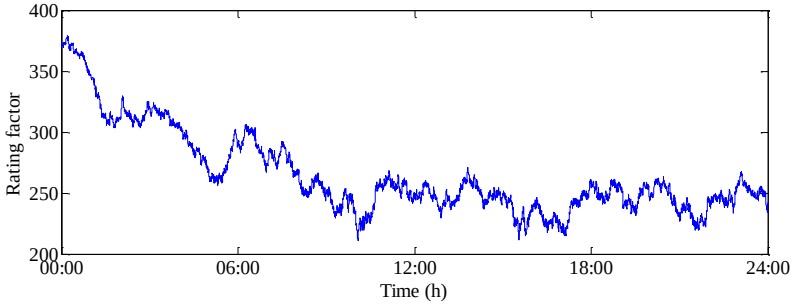

(b) Under weekend light traffic condition

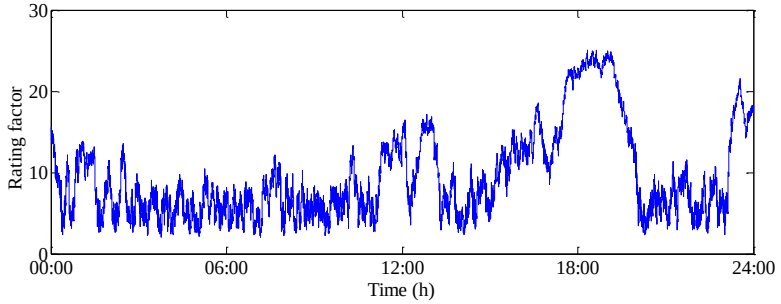

(c) Under typhoon condition

Fig. 13 Daily rating factor under different load conditions

Fig. 14 illustrates the minimum daily rating factor of different sensor installation locations at the quarter-span and mid-span sections from 1 February 2016 to 7 February 2016. It can be seen from Fig. 14 that the critical position at quarter-span section is where the FBG strain sensor STR-G10-8 is deployed and the critical position at mid-span section is where the FBG strain sensor STR-G11-7 is installed. Also, it shows that the rating factors of the mid-span section are more critical than those of the quarter-span section.

5. Conclusions

In this paper, the structural condition of the Jiubao Bridge is evaluated by use of the FBG-based strain monitoring data. A wavelet multi-resolution algorithm is proposed to separate the temperature effect from the raw strain data. The live load-induced stress components under the normal traffic and wind condition and under the typhoon condition are derived. The stress states of different deployment locations and sections are assessed. The structural condition rating of the bridge in accordance with

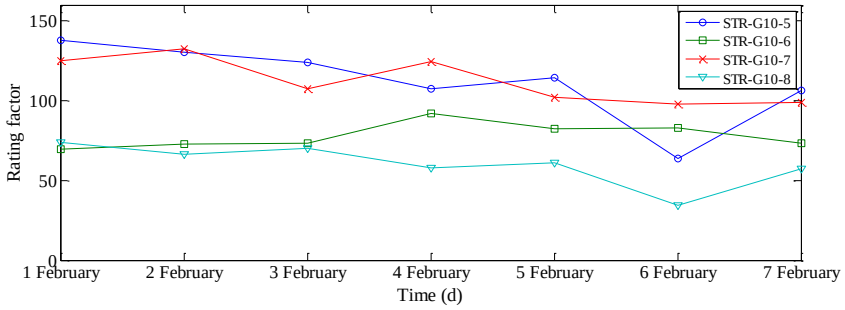

(a) Quarter-span section

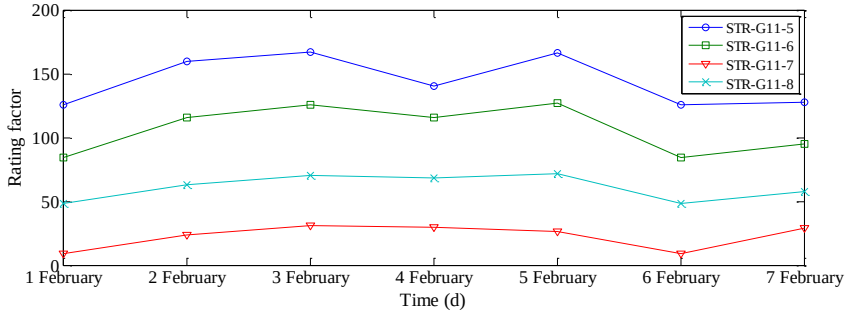

(b) Mid-span section

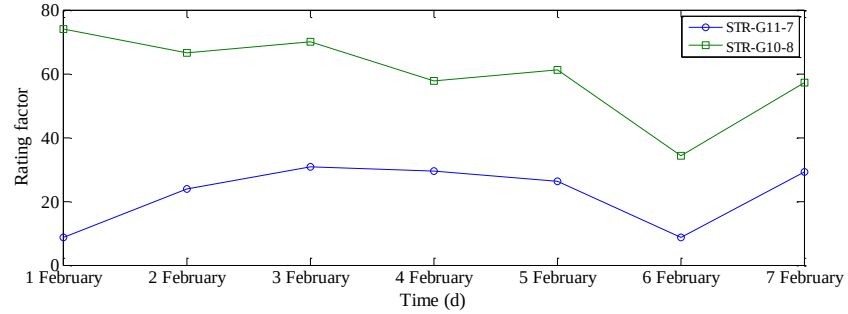

(c) Comparison of STR-G10-8 and STR-G11-7

Fig. 14 Rating factor of quarter-span section and mid-span section

the AASHTO specification for condition evaluation and load resistance and factor rating of highway bridges is performed using the processed data in combination with finite element analysis. The obtained results demonstrate that: (i) the acquired multi-component stress time histories are composed by low frequency signals and high frequency signals which are caused by different kinds of factors, and the wavelet multi-resolution algorithm is an effective tool for decomposing the strain ingredients to achieve the live load-induced stress for further analysis; (ii) the calculated rating factors of selected sections of the Jiubao Bridge under the normal traffic and wind condition and under the typhoon condition are much larger than 1, indicating that the structural components of the bridge are operated in safe condition; and (iii) the analysis framework developed in the present study can be used as a reference for the bridge engineers and managers to schedule and optimize the inspection and maintenance activities of an instrumented bridge.

Acknowledgments

The work described in this paper was jointly supported by the National Natural Science Foundation of China (Grant No. 51625802), the 973 Program (Grant No. 2015CB060000), the Fundamental Research Funds for the Central Universities of China (Grant No. 2017QNA4024), and the Key Lab of Structures Dynamic Behavior and Control (Harbin Institute of Technology), Ministry of Education of the PRC.

References

AASHTO (2011), The Manual for Bridge Evaluation, the 2nd edition. American Association of State Highway and Transportation Officials, Washington DC, USA.

Barbosa, C., Costa, N., Ferreira, L.A., Araujo, F.M., Varum, H., Costa, A., Fernandes, C. and Rodrigues, H. (2008), "Weldable fibre Bragg grating sensors for steel bridge monitoring", *Meas. Sci. Technol.*, **19**(12), 125305.

Cardini, A.J. and DeWolf, J.T. (2008), "Long-term structural

health monitoring of a multi-girder steel composite bridge using strain data", *Struct. Health Monit.*, **8**(1), 47-58.

Casas, J.R. and Cruz, P.J.S. (2003), "Fiber optic sensors for bridge monitoring", *J. Bridge Eng. - ASCE*, **8**(6), 362-373.

Chan, T.H.T., Yu, L., Tam, H.Y., Ni, Y.Q., Liu, S.Y., Chung, W.H. and Cheng, L.K. (2006), "Fiber Bragg grating sensors for structural health monitoring of Tsing Ma bridge: background and experimental observation", *Eng. Struct.*, **28**, 648-659.

Costa, B.J.A. and Figueiras, J.A. (2012), "Fiber optical based monitoring system applied to a centenary metallic arch bridge: design and installation", *Eng. Struct.*, **44**, 271-280.

Fuhr, P.L., Huston, D.R., Nelson, M., Nelson, O., Hu, J. and Mowat, E. (1999), "Fiber optic sensing of a bridge in Waterbury, Vermont", *J. Intel. Mat. Syst. Str.*, **10**(4), 293-303.

Hill, K.O., Fujii, Y., Johnson, D.C. and Kawasaki, B.S. (1978). "Photosensitivity in optical fiber waveguides: Application to reflection filter fabrication", *Appl. Phys. Lett.*, **32**(10), 647-649.

Jiang, G.L., Dawood, M., Peters, K. and Rizkalla, S. (2010), "Global and local fiber optic sensors for health monitoring of civil engineering infrastructure retrofit with FRP materials", *Struct. Health Monit.*, **9**(4), 309-322.

Kister, G., Badcock, R.A., Gebremichael, Y.M., Boyle, W.J.O., Grattan, K.T.V., Fernando, G.F. and Canning, L. (2007a), "Monitoring of an all-composite bridge using Bragg grating sensors", *Constr. Build. Mater.*, **21**(7), 1599-1604.

Kister, G., Winter, D., Badcock, R.A., Gebremichael, Y.M., Boyle, W.J.O., Meggitt, B.T., Grattan, K.T.V. and Fernando, G.F. (2007b), "Structural health monitoring of a composite bridge using Bragg grating sensors. Part 1: evaluation of adhesives and protection systems for the optical sensors", *Eng. Struct.*, **29**(3), 440-448.

Li, H., Ou, J.P., Zhao, X.F., Zhou, W.S., Li, H.W. and Zhou, Z. (2006), "Structural health monitoring system for the Shandong Binzhou Yellow River Highway Bridge", *Comput.-Aided Civ. Inf.*, **21**(4), 306-317.

Mehrani, E., Ayoub, A. and Ayoub, A. (2009), "Evaluation of fiber optic sensors for remote health monitoring of bridge structures", *Mater. Struct.*, **42**(2), 183-199.

Ni, Y.Q., Ye, X.W. and Ko, J.M. (2010), "Monitoring-based fatigue reliability assessment of steel bridges: analytical model and application", *J. Struct. Eng. - ASCE*, **136**(12), 1563-1573.

Ni, Y.Q., Xia, H.W., Wong, K.Y. and Ko, J.M. (2012a), "In-service condition assessment of bridge deck using long-term monitoring data of strain response", *J. Bridge Eng. - ASCE*, **17**(6), 876-885.

Ni, Y.Q., Ye, X.W. and Ko, J.M. (2012b), "Modeling of stress spectrum using long-term monitoring data and finite mixture distributions", *J. Eng. Mech. - ASCE*, **138**(2), 175-183.

Rodrigues, C., Cavadas, F., Felix, C. and Figueiras, J. (2012), "FBG based strain monitoring in the rehabilitation of a centenary metallic bridge", *Eng. Struct.*, **44**, 281-290.

Surre, F., Sun, T. and Grattan, K.T. (2013), "Fiber optic strain monitoring for long-term evaluation of a concrete footbridge under extended test conditions", *IEEE Sens. J.*, **13**(3), 1036-1043.

Tennyson, R.C., Mufti, A.A., Rizkalla, S., Tadros, G. and Benmokrane, B. (2001), "Structural health monitoring of innovative bridges in Canada with fiber optic sensors", *Smart. Mater. Struct.*, **10**(3), 560-573.

Xia, H.W., Ni, Y.Q., Wong, K.Y. and Ko, J.M. (2012), "Reliability-based condition assessment of in-service bridges using mixture distribution models", *Comput. Struct.*, **106-107**, 204-213.

Xiong, W., Cai, C.S. and Kong, X. (2012), "Instrumentation design for bridge scour monitoring using fiber Bragg grating sensors", *Appl. Optics*, **51**(5), 547-557.

Ye, X.W., Ni, Y.Q., Wong, K.Y. and Ko, J.M. (2012), "Statistical analysis of stress spectra for fatigue life assessment of steel bridges with structural health monitoring data", *Eng. Struct.*, **45**, 166-176.

Ye, X.W., Ni, Y.Q., Wai, T.T., Wong, K.Y., Zhang, X.M. and Xu, F. (2013), "A vision-based system for dynamic displacement measurement of long-span bridges: algorithm and verification", *Smart Struct. Syst.*, **12**(3-4), 363-379.

Ye, X.W., Su, Y.H. and Han, J.P. (2014), "Structural health monitoring of civil infrastructure using optical fiber sensing technology: A comprehensive review", *Sci. World J.*, **2014**, Article ID 652329, 1-11.

Ye, X.W., Dong, C.Z. and Liu, T. (2016a), "Image-based structural dynamic displacement measurement using different multi-object tracking algorithms", *Smart Struct. Syst.*, **17**(6), 935-956.

Ye, X.W., Su, Y.H., Xi, P.S., Chen, B. and Han, J.P. (2016b), "Statistical analysis and probabilistic modeling of WIM monitoring data of an instrumented arch bridge", *Smart Struct. Syst.*, **17**(6), 1087-1105.

Ye, X.W., Dong, C.Z. and Liu, T. (2016c), "Force monitoring of steel cables using vision-based sensing technology: methodology and experimental verification", *Smart Struct. Syst.*, **18**(3), 585-599.

Ye, X.W., Liu, T. and Ni, Y.Q. (2017), "Probabilistic corrosion fatigue life assessment of a suspension bridge instrumented with long-term SHM system", *Adv. Struct. Eng.*, DOI: 10.1177/1369433217698345.

Zhang, W., Gao, J.Q., Shi, B., Cui, H.L. and Zhu, H.H. (2006), "Health monitoring of rehabilitated concrete bridges using distributed optical fiber sensing", *Comput.-Aided Civ. Inf.*, **21**(6), 411-424.

Zhou, G.D., Yi, T.H. and Chen, B. (2016), "Innovative design of a health monitoring system and its implementation in a complicated long-span arch bridge", *J. Aerospace Eng. - ASCE*, B4016006, 1-17.